ELSEVIER

Materials Science and Engineering A 485 (2008) 581–588

MATERIALS SCIENCE & ENGINEERING A

www.elsevier.com/locate/msea

Study of texture and microtexture during β to α + β transformation in a Ti–5Ta–1.8Nb alloy

T. Karthikeyan [a], Arup Dasgupta [a], S. Saroja [a,*], R. Khatirkar [b,1], M. Vijayalakshmi [a], I. Samajdar [b]

[a] *Physical Metallurgy Division, Metallurgy and Materials Group, Indira Gandhi Centre for Atomic Research, Kalpakkam 603102, India*
[b] *Department of Metallurgical Engineering and Materials Science, IIT Bombay, Mumbai 400076, India*

Received 29 June 2006; received in revised form 9 August 2007; accepted 20 August 2007

Abstract

This paper discusses the evolution of texture in a Ti–5Ta–1.8Nb alloy during the transformation of 'deformed α + β → β → α + β', characterized using X-ray diffraction and Electron Back Scattered Diffraction techniques. It exhibited a deformation texture of type—[1 0 −1 0]//axial direction (AD) for the wire, and a [0 0 0 2]//normal direction (ND) for the cold rolled sheet sample. On subsequent β-homogenization treatment and cooling, the initial deformation texture was replaced with a transformation texture of [1 1 −2 0]//ND for the sheet sample. The wire sample exhibited a transformation texture with (1 1 −2 2) aligned near to the wire cross-section. A deformation texture was found to be essential to introduce transformation texture.

Keywords: Titanium alloys; Phase transformation; X-ray diffraction; Electron back scatter diffraction and microtexture

1. Introduction

Titanium alloys possess a good combination of weight, strength, toughness, and corrosion resistance and find a broad spectrum of applications in chemical [1], biomedical [2] and nuclear [3] industries. This is achieved through appropriate design of microstructures, as a result of a host of phase transformations in these alloys [4–6]. The transformation mechanism of high temperature bcc β phase is highly sensitive to the composition of the alloy and the cooling rate [7]. Titanium alloys can either be α (hcp), α + β (hcp + bcc) or β (bcc)—the α + β type being the most preferred due to the best combination of strength and toughness. Addition of refractory metals, such as, tantalum and niobium to titanium has been reported to decrease the β transus temperature (T_β), widen the two-phase (α + β) regime [8,9], improve the corrosion resistance in nitric acid in addition to imparting better mechanical formability behavior [10,11].

HCP metals, such as Ti, Zr and their alloys exhibit strong tendencies to develop textures during forming operations, recrystallization and phase transformation [12–14]. It is known that crystal properties like anisotropy of the lattice, stacking fault energy, *c*/*a* ratio and processing parameters like temperature, mode and extent of deformation and strain rate dictate the deformation texture in an alloy. Also, the transformation β → α in Ti systems generally obeys the following Burgers crystallographic orientation relationship (BOR) [15]: $\{1\,1\,0\}_\beta//\{0\,0\,0\,1\}_\alpha$ and $\langle 1\,1\,1\rangle_\beta//\langle 1\,1\,-2\,0\rangle_\alpha$.

Gey and Humbert [16] had reported that when commercially pure Ti (CP, purity ∼99.85%) is β annealed after unidirectional deformation (such as cold rolling), the β phase inherits a strong $\{1\,1\,2\}\langle 1\,1\,1\rangle$ type of texture, while no specific β phase texture was observed when there was no initial cold rolling. Gey and Humbert [16] have also reported a $\{1\,0\,-1\,3\}\ \langle 1\,-2\,1\,0\rangle$ type of texture after a β → α transformation for an initially rolled titanium and a nearly random α product when not subjected to the initial rolling. In other words, the type of texture that develops in the product α phase during the transformation, 'deformed α → β → α', is governed by the texture of parent β phase, which in turn depends on the deformation texture in the parent α phase. However, evaluation of the high temperature β phase texture involves either very special experimental technique, such as in

* Corresponding author. Tel.: +91 44 27480306; fax: +91 44 27480202.
E-mail address: saroja@igcar.gov.in (S. Saroja).
[1] Present address: Department of Metallurgical and Materials Engineering, Visvesvaraya National Institute of Technology, Nagpur-440011, India.

0921-5093/$ – see front matter © 2007 Elsevier B.V. All rights reserved.
doi:10.1016/j.msea.2007.08.042

situ hot stage electron back-scattered diffraction (EBSD) [17] or computational methods, where assuming that BOR is obeyed, the prior β texture is deduced from the texture of product α phase [16,18,19].

It is known that deformation texture in Ti may be altered by addition of alloying elements. Extensive literature [13,14,20–22] is available to confirm the various types of textures that develop in titanium alloys, depending on the alloy chemistry and thermo-mechanical treatments. It has been reported in Ti binary alloys, that, addition of Ta (<15 wt.%) or Nb (<3.6 wt.%) has little effect upon the α-deformation texture of a cold-rolled sheet [13]. However, literature on textures developed in Ti–Ta–Nb ternary alloy systems is very scarce. Recently, the study of transformation texture in a wire drawn Ti–5Ta–1.8Nb alloy [23] has been reported by us. This alloy has excellent corrosion resistance, good formability and weldability characteristics. Hence, it is being considered as an alternative to the presently used commercial Ti grades and stainless steels for applications in highly corrosive media. The commercial exploitation of this alloy largely depends on successful fabrication into various shapes such as sheets, tubes and wires. Understanding of the microstructure and texture that develop in this alloy during deformation and heat treatment is, therefore, crucial. Hence, an extensive experimental investigation has been carried out to study the texture that develops in α-β Ti–Ta–Nb system, during room temperature deformation and the subsequent transformation of the high temperature β phase during cooling. This study also aims to elucidate the texture evolution on a microscopic scale and the orientation relationships between the parent and product phases in a $\beta \rightarrow \alpha + \beta$ transformation. The present paper deals with two aspects of the Ti–5Ta–1.8Nb alloy, namely: (i) development of deformation texture by different methods of cold deformation like cold rolling and wire drawing and (ii) influence of deformation texture on the subsequent transformation texture of a deformed $\alpha \rightarrow \beta \rightarrow \alpha + \beta$ system.

2. Experimental

The Ti–5Ta–1.8Nb alloy in the form of wires of 1.6 mm in diameter was supplied by Nuclear Fuel Complex, Hyderabad, India [24]. The chemical composition of the alloy is given in Table 1. These wires were cold rolled to sheets of 0.26 mm in thickness and 3.2 mm in width. The cold rolling, which was nearly 83% was unidirectional and completed in four passes without any intermediate stress relieving treatments. The rolled sheets were vacuum-sealed ($\sim 10^{-5}$ Torr) in quartz tubes. The samples were solution treated for 2 h at 1273 K in the β phase field and then cooled to room temperature by slow cooling (SC) at a rate of 0.03 K/s.

Table 1
Chemical composition of the Ti–Ta–Nb alloy

Element	Alloy elements (in wt.%)		Impurities (in ppm)					Ti
	Ta	Nb	Fe	O	N	C	H	
Content	4.39	1.94	263	501.5	47	125	9	Balance

Specimens for metallography were prepared by standard preparation procedures. The final polishing was done using 0.25 μm alumina slurry followed by etching using Krolls reagent. Optical metallography was carried out using a Leica MEF4A optical microscope. X-ray diffraction (XRD) studies were carried out by a Philips PW-1730 X-ray diffractometer using Cu Kα radiation on the alloy strips and powdered TiTaNb, which will henceforth be referred to as the 'powder' pattern for this alloy. The crystallographic orientation of the microstructural constituents (referred to as microtexture in this paper) from a selected region of a specimen was studied using Electron Back Scattered Diffraction (EBSD) technique in a FEI Quanta 200 HV Scanning Electron Microscope, attached with a PEGASUS-EBSD analyzer. A final electropolishing using an electrolyte of 20% perchloric acid in methanol, at −25 °C, for 45 s was employed to obtain the strain-free specimen surface, suitable for EBSD studies. The microtexture studies were performed on the flat rolling plane for the sheet samples and on the cross-section for the wire specimen.

3. Results

This section presents the results on the texture that develops in cold rolled Ti–5Ta–1.8Nb alloy during 'deformed-$\alpha + \beta \rightarrow \beta \rightarrow \alpha + \beta$' transformation, when the high temperature β phase is slow cooled. These results are compared with that of specimen with a different deformation history such as wire drawing and one that has no prior history, i.e., cooled from liquid phase.

3.1. Microstructural characterization of initial and heat treated alloy

The optical micrographs of the initial wire and cold rolled alloy are shown in Fig. 1(a and b). A microstructure characteristic of a heavy deformation showing elongated grains aligned along the wire axis and rolling direction is seen. The presence of β phase could not be identified due to their low fraction and size. The microstructure obtained after heat treatment in β phase field and slow cooling is shown in Fig. 2, which is completely different from the initial one. A well defined lamellar α and β structure along with Grain Boundary α (GB-α) [8,23] is observed. Usually such transformation products in Ti alloys are also accompanied by development of texture, which is described in the subsequent sections.

Fig. 3(a) shows the secondary electron micrograph of a weld region, obtained by a manual gas tungsten arc welding (GTAW) process, details of which are given elsewhere [25]. The microstructure shows a typically martensitic product. It is important to mention that the alloy has undergone two transformations, namely Liquid → β, followed by a solid state transformation $\beta \rightarrow \alpha'$ and hence does not possess any history of deformation. The faster cooling rates during the β transformation lead to the martensitic α' instead of a Widmanstätten product. Fig. 3(b) shows the X-ray diffraction pattern from the weld sample. The peak positions and relative intensities closely match with the JCPDS data for α-Ti [26], suggesting the absence of any preferred orientations.

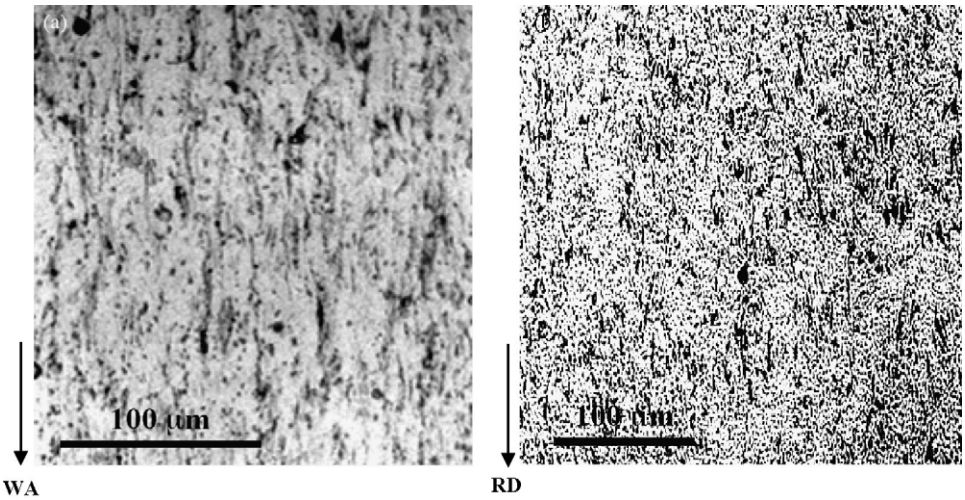

Fig. 1. Optical micrograph of Ti–5Ta–1.8Nb alloy. (a) L–D section of wire showing a fragmented grain structure, with grains elongated along the wire axis (WA) and (b) alloy subjected to 83% unidirectional cold rolling showing a similar structure but with severe deformation (RD indicates the rolling direction).

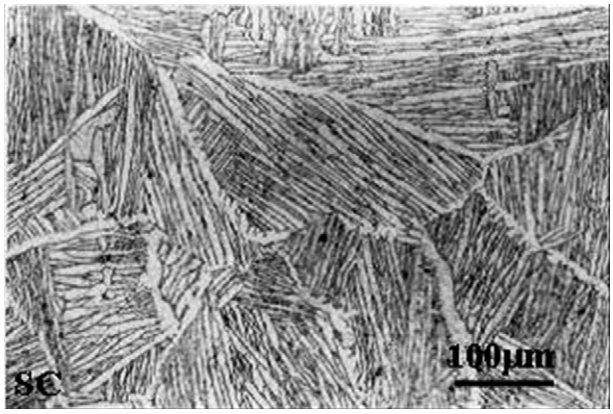

Fig. 2. Optical micrograph showing the decoration of grain boundary α on prior β boundaries with coarse lamellae of α and β in Ti–5Ta–1.8Nb alloy obtained by slow cooling (SC) during β → α transformation.

3.2. Study of texture developed in Ti–Ta–Nb alloy

The deformation and transformation textures exhibited by the Ti–5Ta–1.8Nb alloy have been studied by X-ray diffraction and EBSD techniques. Crystals with plane normal coinciding with the sample normal are detected in the θ–2θ geometry by XRD. Therefore, the observation of an unusually high intensity of a peak whose structure factor is otherwise low, together with reduction of intensities of other peaks is a signature of crystallographic texture. Since XRD studies using θ–2θ geometry does not give a complete description of texture in a material, texture of microscopic constituents (microtexture) has been carried out using EBSD.

3.2.1. Texture analysis by XRD

3.2.1.1. Study of deformation texture in the Ti–Ta–Nb alloy. The XRD patterns from the (length–width) surface section of cold rolled and cross-section of the wire are shown in Fig. 4, along with the XRD 'powder' pattern as reference. The intensities are normalized with respect to the peak with maximum intensity. It is observed that the most intense peak in the powder pattern corresponds to $(1\,0\,-1\,1)_\alpha$. The relative peak intensities are in agreement with the JCPDS data for α-Ti [26], except the peak at 38.4°, which shows an enhancement in intensity. This enhancement is attributed to the overlap from $(1\,1\,0)_\beta$ of 100% intensity [27], which also confirms the α-β nature of the alloy.

In contrast to the powder sample, the relative peak intensities for the deformed samples are significantly different. The

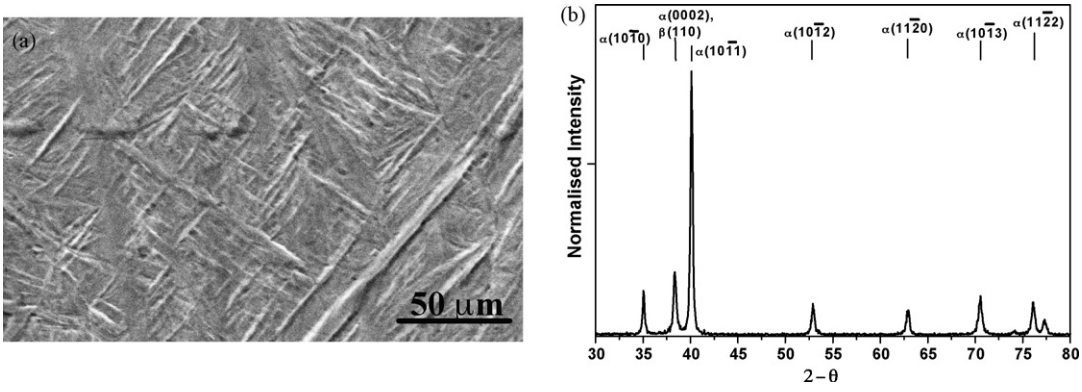

Fig. 3. (a) SEM micrograph of a weld showing a typical martensitic structure and (b) XRD pattern using Cu Kα incident radiation showing a nearly powder pattern.

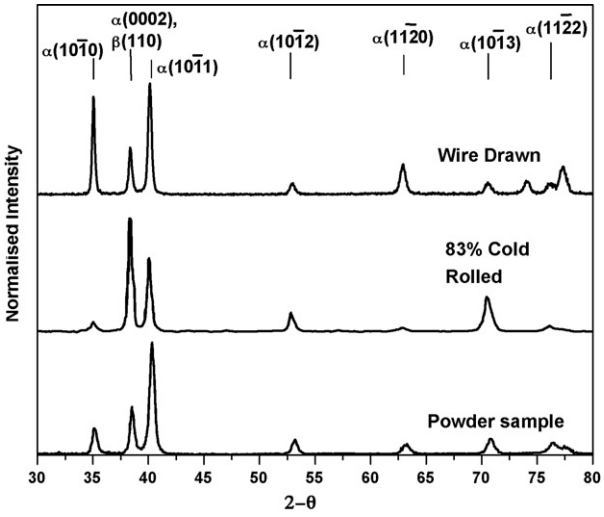

Fig. 4. XRD patterns showing the resultant deformation texture with two different modes of deformation, namely unidirectional cold rolling (83% reduction) and wire drawing. These are compared with the powder pattern.

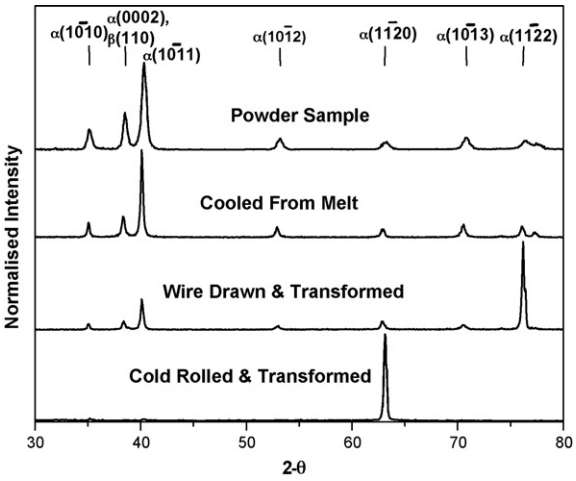

Fig. 5. XRD patterns from products of $\beta \rightarrow \alpha + \beta$ transformation in TiTaNb with different histories, such as cold rolling, wire drawing and melting. Comparison with the powder pattern highlights the influence of prior deformation textures on the transformation texture.

strongest (100%) peak for the cold rolled sample is seen at 38.4°, which corresponds to $(0\,0\,0\,2)_\alpha$ as well as $(1\,1\,0)_\beta$ [27], whereas the 100% peak for the powder sample is at 40.1° corresponding to $(1\,0\,-1\,1)_\alpha$. The low amount of β phase precludes a significant contribution from the $(1\,1\,0)_\beta$ peak. Therefore, the observed change indicates a preferential orientation of α grains during deformation and may be referred to as the 'deformation texture'. The wire drawn sample shows maximum enhancement of peak intensity for a different crystallographic plane, namely $(1\,0\,-1\,0)_\alpha$ [23]. The above results indicate that the alloy acquires deformation textures dictated by the mode of deformation, which in turn depends on the nature of applied stress.

3.2.1.2. Effect of deformation texture on the $\beta \rightarrow \alpha + \beta$ transformation texture. The XRD patterns of the alloy with three different histories such as (a) cold rolled (length–width section), (b) wire drawn (cross-section) and (c) weld are shown in Fig. 5. Of these, the weld specimen does not posses any deformation history. The XRD pattern from the powder sample is also included in this figure, for comparison. It is seen that the single strongest peak is $(1\,1\,-2\,0)_\alpha$ for the cold rolled and transformed (CRT) alloy, while it is $(1\,1\,-2\,2)_\alpha$ for the wire drawn and transformed (WDT) alloy. This is in sharp contrast to the deformation texture observed prior to heat treatment (Fig. 4). The weld exhibits a near powder pattern. This observation of a unique peak in the CRT and WDT samples at 2θ values with minor structure factors is an indication of preferential crystallographic orientation—hereafter referred to as the 'transformation texture'.

The conventional XRD studies in θ–2θ geometry give only qualitative information on the type of texture. Further, "microtexture" studies in the CRT and WDT specimen were carried out to measure quantitatively the texture components and to evaluate the microtexture mechanism, which are described in the subsequent sections.

3.2.2. Study of micro-texture using EBSD technique

3.2.2.1. Analysis of microtexture in the WDT alloy. It was seen earlier from the XRD study on the cross-section of the WDT sample (Fig. 5) that a strong $(1\,1\,-2\,2)_\alpha$ peak appeared, suggesting a transformation texture of type $(1\,1\,-2\,2)_\alpha$ aligned parallel to the wire cross-section. An EBSD scan of the sample was carried out on the wire cross-section to evaluate its microtexture and to corroborate the results with the XRD information. It may be mentioned here that only the orientations of the α-colonies of transformed β structure and the GB-α were studied, since α is the major phase in the alloy.

Fig. 6(a) shows the selected area crystal orientation map (SACOM), depicting the type of crystallographic plane that are aligned with the sample surface, i.e., wire cross-section; Fig. 6(b) gives the color index for reading the grain orientation map. The α lamellas within the colony share a common crystallographic orientation. The GB-α phases share the orientation with one of its neighboring colony, and thus, do not show as a separate grain in the map. Two types of color concentrations, namely light green and red are observed in the region.

The orientation data was analyzed to calculate the inverse pole figure distribution for the axial direction, which is shown in Fig. 6(c). The pole normals corresponding to the planes of α-Ti that have significant peak intensities in XRD-powder pattern, such as $(1\,0\,-1\,1)$, $(0\,0\,0\,1)$, $(1\,0\,-1\,0)$, $(1\,0\,-1\,2)$, $(1\,1\,-2\,0)$, $(1\,0\,-1\,3)$ and $(1\,1\,-2\,2)$ are labeled in the figure. Two pole concentrations are observed, with the maximum intensity as 3.012. The concentrations are not seen to be centered exactly on any of the known crystallographic directions or the crystallographic plane normals mentioned above. However, the $(2\,-1\,-1\,2)$ plane normal is seen to be close (~8°) to the primary concentration. Apart from this, no other simple $(h\,k\,i\,l)$ plane normals is observed to lie close to this primary concentration. This is accordance with the XRD results where a strongest intensity of $(1\,1\,-2\,2)_\alpha$ peak, and weak intensity of the other $(h\,k\,i\,l)$ peaks was observed. The EBSD results show that the crystallographic

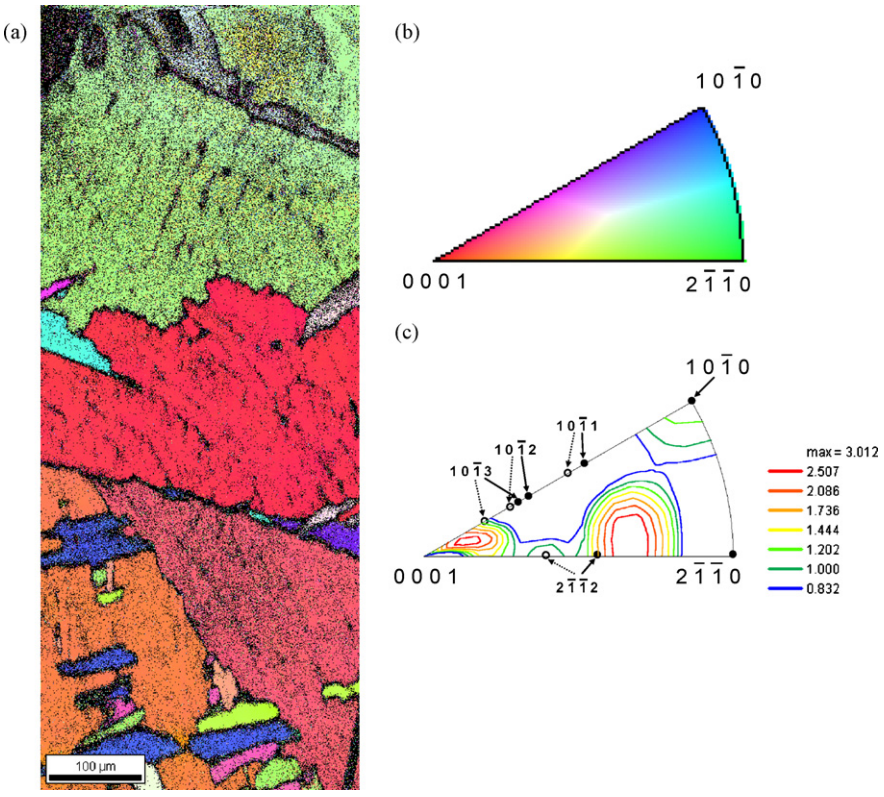

Fig. 6. (a) SACOM of the cross-section of the wire sample illustrating the type of plane aligned with the wire cross-section (b) color Index for the SACOM and (c) inverse pole figure for the wire axial direction depicting two near pole concentrations—crystallographic plane normals (closed circles) and directions (open circles) have been labeled. (For interpretation of the references to color in this figure legend, the reader is referred to the web version of the article).

plane that preferentially align with the wire cross-section is not exactly the (1 1 −2 2), but some plane with irrational indices close to it. In the inverse pole figure (Fig. 6c), another concentration near to the [0 0 0 1] is observed. Again, no (*h k i l*) plane satisfying XRD conditions occur near this concentration, and even the (0 0 0 1) normal is seen to occur only at the periphery contour of relatively low intensity. Hence, this component of texture was evident only as a weak peak in the XRD analysis (Fig. 5).

3.2.2.2. Analysis of microtexture in the CRT alloy. The phase identification map for α- and β-Ti from a selected area in the CRT sample is shown in Fig. 7(a), where they have been distinguished by different color codes (red and white, respectively). The fine size of lamellar β-Ti phase is almost at the limit of detection of the EBSD probe, which is ∼0.2 μm. Thus, the fraction of β phase identified in the phase identification map is an under estimation of its volume fraction. The corresponding SACOM is shown in Fig. 7(b), where the various orientations of α and β-Ti are shown in shades of green and blue, respectively. A careful examination of the figures reveals the presence of a GB-α region, suggesting the presence of an intervening prior β grain boundary. This implies that the mapped α + β phases have transformed from two different β grains, say β1 and β2. The product α-lamellae from β1 and β2 are marked as $\alpha_{\beta 1}$ and $\alpha_{\beta 2}$, respectively. It is observed that within each of the two parent β grains, majority of α lamellae possesses a similar orientation. Similar feature is also observed for the β lamellae, although all of the β lamellae could not be crystallographically indexed owing to their fine size, as explained earlier. The α orientation also remains unchanged across the two β grains. The presence of α lamellae with similar crystallographic orientation on either side of the prior β grain boundary is also a signature of preferential orientation in the alloy. The crystallographic analysis of the room temperature β phase could provide valuable information about the high temperature β texture. Hence, detailed crystallographic analysis has been carried out for α and β phases, using pole figures. In literature, however, the analysis of the β phase has mainly been done either through numerical calculations [16,18,19] or high temperature EBSD [17].

Identification of poles along major crystallographic axes corresponding to the individual α and β phases in the selected area has been carried out by analysis of the EBSD data. Accordingly, the poles corresponding to $\alpha_{\beta 1}$ and $\alpha_{\beta 2}$ and β1 and β2 are marked in Fig. 8(a and b), respectively. Fig. 8(a) shows the pole density contours for the (0 0 0 2) and (1 1 −2 0) plane normal of hcp α-Ti phase corresponding to the SACOM in Fig. 7(b). A dense concentration of (0 0 0 2) poles along the rolling direction (RD) and (1 1 −2 0) along the sample normal direction (ND) is seen in this figure. The alignment of α lamellae with (1 1 −2 0) plane normal oriented along the sample normal is in good agreement with the XRD data (Fig. 5). In addition, for the (1 1 −2 0) a pair of pole concentrations at an angle of about 60° between the ND and cross-direction (TD) was also observed. However, all the three pole concentrations for the (1 1 −2 0) plane normal

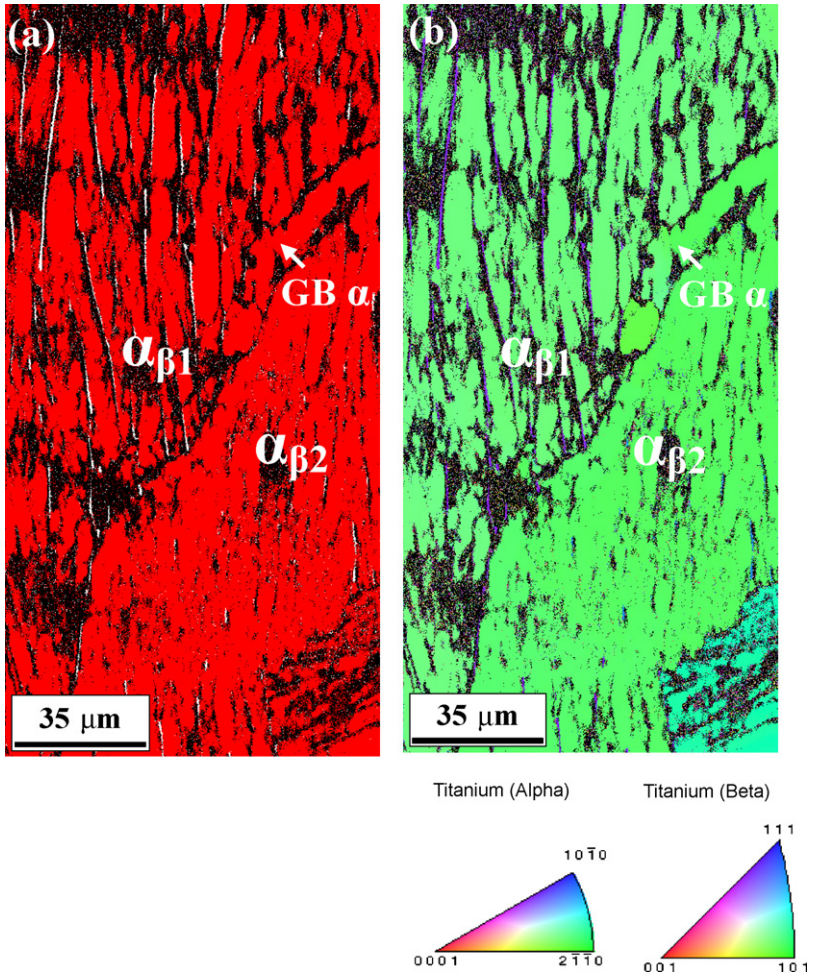

Fig. 7. EBSD images in an alloy solutionized in β phase field and slow cooled (a) phase identification map for α- and β-Ti phases (color coded as red and white, respectively) and (b) crystal orientation map of α- and β-Ti (coded as green and blue). GB-α denotes grain boundary α, which demarcates the boundary between two parent β grains and $\alpha_{\beta1}$ and $\alpha_{\beta2}$ denote α phases that evolved from the prior β grains β1 and β2, respectively. (For interpretation of the references to color in this figure legend, the reader is referred to the web version of the article.)

can be attributed to the same set of lamellae, based on symmetry considerations, suggesting that $\alpha_{\beta1}$ and $\alpha_{\beta2}$ have identical orientation.

Fig. 8(b) shows the pole density contours along the (1 1 1) and (1 1 0) plane normals of the retained bcc β-Ti phase, corresponding to the SACOM in Fig. 7(b). From symmetry consideration, each β grain would give rise to four (1 1 1) pole concentrations. In the present case, two sets of such pole concentrations are observed, of which three form a triangle with the fourth nearly at the centre. The two triangles have been identified and marked in the figure. It is seen that the central pole is common to both triangles and almost coincides with the centre of the pole figure, i.e., along ND. It is also seen that one of the triangles is rotated with respect to the other by an angle Ω about the central (1 1 1) pole. Similarly, for the pole figure corresponding to (1 1 0), the (1 1 0) plane normal would give rise to six pole concentrations. Again two sets of β crystals can be identified, one aligned along the rolling direction and another tilted away from it. The absence of a peak corresponding to $(1\,1\,1)_\beta$ plane in XRD pattern can be understood in terms of the very low relative intensity of the $(2\,2\,2)_\beta$ peak due to high values of 2θ ($\sim$107° with Cu Kα radiation).

The above results have shown that orientations for $\alpha_{\beta1}$ and $\alpha_{\beta2}$ nearly overlap with one another while those for β1 and β2 are inclined by an angle Ω with respect to one another. The α crystals are aligned in such a way that their basal plane $(0\,0\,0\,2)_\alpha$ normal lies along the rolling direction and the $(1\,1\,-2\,0)_\alpha$ plane normal lies along the ND. On the other hand, the β crystals are aligned in such a way that for both β1 and β2, one of the (1 1 1) plane normal is parallel to one another and are aligned along the ND. However, the misorientation between these two crystals is such that β1 crystals have their (1 1 0) plane normal aligned along the RD, while β2 crystals have them tilted from the RD by an angle Ω.

The results described so far can be summarized as follows: (i) deformation texture exhibited by Ti–Ta–Nb alloy was dependent on the mode of deformation, $(0\,0\,0\,2)_\alpha$ for cold rolled and $(1\,0\,-1\,0)_\alpha$ for wire drawing, which were completely altered during the subsequent $\beta \rightarrow \alpha + \beta$ transformation, (ii) a prior deformation history is essential to obtain a textured transformed

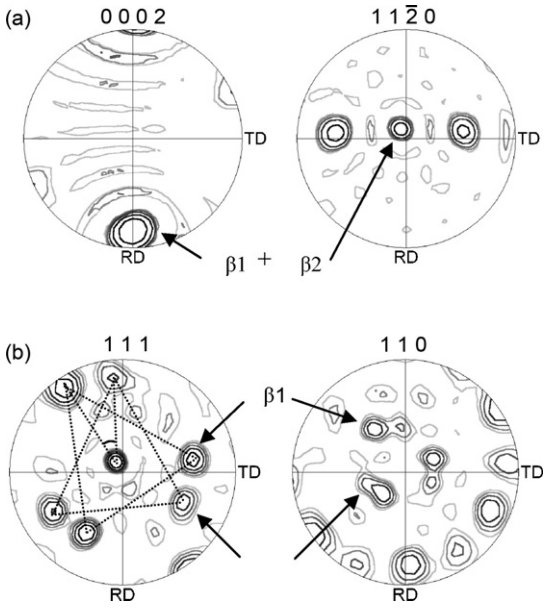

Fig. 8. Pole figure contours computed from the SACOM. (a) Pole concentrations along (0 0 0 2) and (1 1 −2 0) plane normals for α-Ti phase and (b) pole concentrations along the (1 1 1) and (1 1 0) plane normals for the β-Ti phase.

product which was confirmed in a sample cooled from liquid and (iii) EBSD results showed that product α had the same orientation although the two adjacent parent β grains had different orientations.

4. Discussion

The observed deformation and transformation textures are summarized in Table 2. The basal plane $(0\,0\,0\,2)_\alpha$ type of deformation textures have been reported for cold rolled Ti and other hcp metals [13,28,29]. The wire texture of $(1\,0\,-1\,0)_\alpha$ aligned with the wire cross-section, or in other words, $[1\,0\,-1\,0]_\alpha$//AD has also been reported in titanium [30] and zirconium alloys [31]. Gey et al. [31] have observed a wire transformation texture of $[1\,1\,-2\,0]_\alpha$//AD in the zirconium alloy. Zeng and Bieler [30] have reported a fiber transformation texture with $[0\,0\,0\,2]_\alpha$ aligned parallel to the axial direction in Ti alloy. In contrast, in the present study, EBSD microtexture of the wire cross-section showed two texture components, one close to the $(1\,1\,-2\,2)_\alpha$ and another near to the $(0\,0\,0\,2)_\alpha$.

Widmanstätten transformation demands the cooperative growth of α lamellae [32]. In Ti alloys this transformation results in crystallographically aligned α, which introduces microtexture within α colonies [23,33]. During the transformation, the GB-α is the first product to form [34]. Next, to form are the colonies of lamellar α, which nucleate along the GB-α and grow into the β grains. It was shown in our earlier study [23] that the orientation of the GB-α is same as that of the neighboring α colonies within the parent β grain.

The present study showed the importance of prior deformation to obtain a textured transformed product. Whether cold rolled or wire drawn, the final transformed product was textured. But the nature of transformation texture, viz., $(1\,1\,-2\,0)_\alpha$ for the cold rolled and a $(1\,1\,-2\,2)_\alpha$ component for the wire drawn sample indicated that transformation texture is dictated by the type of deformation texture which are $(0\,0\,0\,2)_\alpha$ for the former and $(1\,0\,-1\,0)_\alpha$ for the latter. The above results together with the observed random orientations when cooled from liquid state suggest that an initial deformation is essential to obtain a textured transformation product. This is because Burgers Orientation Relation [15] is obeyed in Ti alloys [16,17,34] both during the $\alpha+\beta\rightarrow\beta$ and $\beta\rightarrow\alpha+\beta$ transformations, during heating and cooling, respectively. Thus, a unique deformation texture results in a unique texture for the high temperature β phase, which in turn decomposes into product α phase following BOR, which introduces transformation texture in the products.

The SACOM pattern from EBSD analysis of CRT specimen has clearly shown that two adjoining prior β grains (β1 and β2) share a common (1 1 0) plane giving rise to an (1 1 −2 0) orientation for the GB-α and α colonies on either side of the parent β/β boundary. As described in the previous section, the two β's are misoriented with respect to each another by an angle Ω, which has been evaluated to be about 31°. The orientation of α is observed to be same within both the prior β grains, despite this misorientation. This suggests that the product α is not affected by the misorientation of its parent grain. Analysis of EBSD pole figures has shown that for the β1 grain, which has the (1 1 0) plane normal aligned along the RD, the following Burgers Orientation Relationship is strictly followed, i.e.,

$$(1\,1\,-2\,0)_{\alpha_1}||(1\,1\,1)_{\beta_1}\text{ and }\langle 0\,0\,0\,2\rangle_{\alpha 1}||\langle 1\,1\,0\rangle_{\beta 1}$$

However, based on observation of similar orientation between α1 and α2, and a misorientation of about ∼31° between β1 and β2, it is reasonable to say that the lamellar transformation product of β2 grain does not strictly follow the BOR stated above. In other words, this is a typical situation wherein the orientation relation between α2 and β2 is such that,

$$(1\,1\,-2\,0)_{\alpha 2}//(1\,1\,1)_{\beta 2}\text{ but }\langle 0\,0\,0\,2\rangle_{\alpha 2}\#\langle 1\,1\,0\rangle_{\beta 2}$$

A similar observation is reported by Bhattacharyya et al. [35] in α + β Ti–6Al–2Sn–4Zr–6Mo alloy when the GB-α to minimize interfacial energy selects $(0\,0\,0\,1)_\alpha||\{1\,1\,0\}_\beta$ such that the specific {1 1 0} is common to both prior β grains. It is necessary to mention here that the orientation of $\alpha_{\beta 1}$, where BOR is obeyed, has prevailed over that of $\alpha_{\beta 2}$, where BOR is only

Table 2
Effect of deformation texture on transformation texture

S. no.	Mode of deformation	α Deformation texture	α Transformation texture
1	Cold rolling	[0 0 0 2]//Normal direction	[1 1 −2 0]//Normal direction
2	Wire drawing	[1 0 −1 0]//Axial direction	Major component close to (1 1 −2 2)//wire cross-section
3	Cooling from melt	Not applicable	None (random)

partially obeyed. This is explained on the basis of the diffusion controlled transformation mechanism that operates in the SC sample. The GB-α nucleates at the prior β/β boundary following BOR for any one of the two β grains (say β1). Further α lamellae growing out of GB-α that has already nucleated with preferential orientation maintains the same orientation although this amounts to deviations from BOR (for β2). This is made possible by the diffusion distances, which are much larger during a diffusional transformation than required for strict adherence to BOR.

5. Conclusion

The influence of initial deformation on the transformation of high temperature $\beta \rightarrow \alpha + \beta$ in a developmental Ti–5Ta–1.8Nb alloy has been studied. The texture that developed during deformation and transformation was studied using XRD and EBSD analysis. The room temperature microstructure of $\beta \rightarrow \alpha + \beta$ transformation product is Widmanstätten α for slow cooling rates and a martensitic α′ for faster cooling rates of welds. Deformation texture developed by the alloy is $[0\,0\,0\,1]_\alpha$//ND for rolling and $[1\,0\,-1\,0]_\alpha$//AD for wire drawing, showing that it depends on the mode of deformation. Deformation texture dictates the final texture during the $\alpha + \beta \rightarrow \beta \rightarrow \alpha + \beta$ transformation—$[1\,1\,-2\,0]$//RD and a $(1\,1\,-2\,2)$//wire cross-section component of transformation textures are obtained corresponding to initial deformation textures of $(1\,1\,-2\,0)_\alpha$ (cold rolled) and $(1\,0\,-1\,0)_\alpha$ (wire drawing), respectively. A prior deformation is essential to obtain the final transformation texture; sample cooled from melt results in a randomly oriented product. Microtextural analysis showed a case where Burgers Orientation Relation is only partly obeyed. This is understood in terms of grain boundary α which being the first to form exerts a strong influence on the orientation of subsequent transformation products.

Acknowledgements

The authors would like to thank Dr. Baldev Raj, Director IGCAR for his keen interest and support for this project. The authors would also like to thank Mr. V. Sankara Sastry of Materials Science Division, IGCAR, for useful discussions and some X-ray diffraction experiments.

References

[1] D. Eylon, ASM Metals Handbook, vol. 2, ASM International, 1990, pp. 634–646.
[2] M. Niinomi, T. Hattori, K. Morikawa, T. Kasuga, A. Suzuki, H. Fukui, S. Niwa, Mater. Trans. 43 (2002) 2877–2970.
[3] B. Raj, U. Kamachi Mudali, T. Jayakumar, K.V. Kasiviswanathan, R. Natarajan, Sadhana 25 (2000) 519–559.
[4] F.J. Gil, M.P. Ginebra, J.M. Manero, J.A. Planell, J. Alloys Compds. 329 (2001) 142–152.
[5] F S Banerjee, IIM (The Indian Institute of Metals) Metal News, vol. 5, 2002, pp. 9–17.
[6] D. Veeraraghavan, P. Wang, V.K. Vasudevan, Acta Mater. 51 (2003) 1721–1741.
[7] T. Ahmed, H.J. Rack, Mater. Sci. Eng. A243 (1998) 206–211.
[8] R. Mythili, V. Thomas Paul, S. Saroja, M. Vijayalakshmi, V.S. Raghunathan, Mater. Sci. Eng. A390 (2005) 299–312.
[9] T.B. Massalski, H. Okamoto, P.R. Subramanian, L. Kacprzak, Binary Alloy Phase Diagrams, second ed., ASM International, 1990.
[10] A. Takamura, K. Arakawa, Y. Moriguchi, in: R.I. Jaffee, N.E. Promisel (Eds.), Proceedings on International conference on Science Technology and Applications of Titanium, Pergamon Press, 1970, pp. 209–216.
[11] M. Geetha, U. Kamachi Mudali, A.K. Gogia, R. Asokamani, B. Raj, Corrosion Sci. 46 (2004) 877–892.
[12] G.E. Dieter, Mechanical Metallurgy, McGraw-Hill Book Company, 1988, pp. 237–240.
[13] F. Larson, Properties of Textured Titanium alloys, Metals and Ceramics Information Center, 1974, p. 8.
[14] A.K. Singh, R.A. Schwarzer, Z. Metallkd. 91 (2003) 702–716.
[15] W.G. Burgers, Physica 1 (1934) 561–586.
[16] N. Gey, M. Humbert, Acta Mater. 50 (2002) 277–287.
[17] G.G.E. Seward, S. Celotto, D.J. Prior, J. Wheeler, R.C. Pond, Acta Mater. 52 (2004) 821–832.
[18] M.G. Glavicic, P.A. Kobryn, T.R. Bieler, S.L. Semiatin, Mater. Sci. Eng. A346 (2003) 50–59.
[19] M.G. Glavicic, P.A. Kobryn, S.L. Semiatin, Mater. Sci. Eng. A385 (2004) 372–376.
[20] S. Zaefferer, Mater. Sci. Eng. A344 (2003) 20–30.
[21] A.K. Singh, R.A. Schwarzer, Mater. Sci. Eng. A307 (2001) 151–157.
[22] S. Shang, J. Shen, X. Wang, Mater. Sci. Eng. A326 (2002) 249–254.
[23] T. Karthikeyan, A. Dasgupta, S. Saroja, M. Vijayalakshmi, A.J. Khan, D. Bhattacharjee, V.S. Raghunathan, Mater. Sci. Eng. A393 (2005) 294–302.
[24] K. Kapoor, V. Kain, T. Gopalkrishna, T. Sanyal, P.K. De, J. Nucl. Mater. 322 (2003) 36–44.
[25] T. Karthikeyan, A. Dasgupta, S. Saroja, M. Vijayalakshmi, J. Mater. Eng. Perform. 14 (2005) 241–248.
[26] JCPDS No. 44-1294.
[27] JCPDS No. 44-1288.
[28] M.J. Philippe, M. Serghat, P. van Houtte, C. Esling, Acta Met. Mater. 43 (1995) 1619–1630.
[29] Z.S. Zhu, J.L. Gu, N.P. Chen, Script. Metall. 30 (1994) 605–609.
[30] L. Zeng, T.R. Bieler, Mater. Sci. Eng. A392 (2005) 403–414.
[31] N. Gey, E. Gautier, M. Humbert, A. Cerqueira, J.L. Bechade, P. Archambault, J. Nucl. Mater. 302 (2002) 175–184.
[32] S.J. Jones, H.K.D.H. Bhadeshia, in: K. Inoue, K. Mukherjee, K. Otsuka, H. Chen (Eds.), International Conference on Displacive Phase Transformations and Their Applications in Materials Engineering, TMS, Warrendale, PA, 1998, pp. 419–426.
[33] D.R. Clarke, in: O. Buck, J.K. Tien, H.L. Marcus (Eds.), Electron and Positron Spectroscopies in Material Science and Engineering, Academic Press Inc., 1979, pp. 315–334.
[34] B. Appolaire, L. Heĭricher, E. Aeby-Gautier, Acta Mater. 53 (2005) 3001–3011.
[35] D. Bhattacharyya, G.B. Viswanathan, R. Denkenberger, D. Furrer, H.L. Fraser, Acta Mater. 51 (2003) 4679–4691.